PERGAMON

International Journal of Heat and Mass Transfer 44 (2001) 3895–3905

International Journal of HEAT and MASS TRANSFER

www.elsevier.com/locate/ijhmt

Flow around a bubble on a heated wall in a cross-flowing liquid under microgravity condition

Avijit Bhunia, Yasuhiro Kamotani *

Department of Mechanical and Aerospace Engineering, Case Western Reserve University, 412 Glennan Building, 10900 Euclid Avenue, Cleveland, OH 44106-7222, USA

Received 21 July 2000; received in revised form 21 December 2000

Abstract

Fluid motion around a bubble placed on a heated wall of a flowing liquid channel is studied under microgravity condition, using a spectral element based two-dimensional numerical model. It is shown that the flow and temperature fields around the bubble are governed by an interaction between thermocapillary and forced convection. An opposing interaction between the two convection mechanisms creates a recirculation cell at the downstream side of the bubble. Channel flow velocity, length of the heated wall before the bubble, and temperature difference between the heated wall and the bulk liquid are shown to be the most important variables. Their effects on the bubble surface temperature, surface velocity, stagnation point on the bubble surface, length of the recirculation cell along the heated wall, and wall heat transfer near the bubble are investigated.

1. Introduction

Two-phase gas liquid thermal control system has been identified as a better alternative to single phase pumped liquid loop [1] to meet the growing power demand for spacecraft thermal management [2]. The main advantage of a two-phase system lies in the large amount of latent heat that is transferred during boiling and condensation. Other space applications involving gas–liquid flow are life support system [3], subcooled boiling in cryogenic storage system, design of thermal bus for the space station, gas–liquid separation process in space, etc. [4]. In view of its widespread current and potential future applications, the study of two-phase flow, especially boiling, in a microgravity environment continues to be an active area of research for many years. Recent review articles have thrown light on the state of understanding of the subject [5,6]. An important fluid mechanics aspect of two-phase flow that has received comparatively much less attention, is the study of liquid motion in the vicinity of an individual bubble. A clear understanding of the flow and temperature fields in the vicinity of a bubble is necessary as they govern the forces acting on the bubble. The forces, in turn, control bubble growth, detachment and consequently the resulting two-phase flow and heat transfer.

In a gas–liquid system, heating or cooling of the liquid container wall induces temperature gradients in the liquid and thus along the free surface of the bubble sticking to the wall. The induced temperature gradient brings in density variation in the liquid, which, coupled with gravity, creates a buoyancy force leading to a natural convection current. In addition, the temperature gradient along the bubble creates a local variation of surface tension, which in turn causes liquid motion on the surface. The surface motion is transmitted into the bulk liquid due to viscosity, thus setting in thermocapillary convection. In the presence of gravity in a terrestrial environment, buoyancy forces due to density variation in the liquid and density difference between gas and liquid tend to overwhelm all other forces. In contrast, under microgravity condition, with greatly reduced buoyancy, thermocapillary convection becomes an important mode of fluid motion. Its importance in materials processing and fluid management in space was emphasized by Ostrach [7].

* Corresponding author. Tel: +1-216-368-6455; fax: +1-216-368-6445.

E-mail address: yxk@po.cwru.edu (Y. Kamotani).

0017-9310/01/$ - see front matter
PII: S0017-9310(01)00032-1

Nomenclature

a	bubble radius at wall, radius of gas injection hole
c_p	specific heat
Ca	capillary number $= \mu_\ell U_{ref}/\sigma$
h	channel height
h_x	heat transfer coefficient at any x location along heated wall
k	thermal conductivity
L	length of the heated wall before front end corner of the bubble
Ma	Marangoni number $= R_\sigma Pr$
Nu_x	Nusselt number at any x location $= h_x a/k$
n^*, t^*	dimensionless coordinates normal and tangential to bubble surface $= n, t/a$
p^*	pressure (p) non-dimensionalized w.r.t ref. pressure $(p_{ref}) = p/p_{ref}$
Pr	Prandtl number of liquid $= \mu_\ell c_{p\ell}/k_\ell$
r^*	bubble radius (r), non-dimensionalized w.r.t a
R_σ	surface tension Reynolds number $= \rho_\ell U_{ref} a/\mu_\ell$
Re_{loc}, Re_L	Reynolds number, based on U_{loc}, a $(= \rho_\ell U_{loc} a/\mu_\ell)$ and U_{loc}, L $(= \rho_\ell U_{loc} L/\mu_\ell)$
T	temperature
T^*	dimensionless temperature $= (T - T_m)/\Delta T$
$\mathbf{u}^*$	velocity vector ($\mathbf{u}$), non-dimensionalized by U_{ref}
$u^*_{n,t}$	dimensionless velocity normal and tangential to bubble surface $= u_{n,t}/U_{ref}$
$u^+_{x,y}$	dimensionless velocity in the x- and y-direction, non-dimensionalized by U_{av}
U_{av}	average channel (cross) flow velocity
$U^*_{c,max}$	maximum channel flow velocity ($U_{c,max}$), non-dimensionalized by U_{ref}
U_{loc}	local channel (cross) flow velocity at bubble height $a = 6U_{av}[(a/h) - (a/h)^2]$
U_{ref}	reference thermocapillary velocity $= \sigma_T \Delta T/\mu_\ell$
$\bar{V}$	velocity ratio $= U_{ref}/U_{loc}$
V_s^+	bubble surface velocity (V_s) non-dimensionalized by $U_{loc} = V_s/U_{loc}$
x^*, y^*	dimensionless x and y coordinate non-dimensionalized by a
X^*_R	length of recirculation cell along heated wall $= X_R/a$
X^*_s	dimensionless X location of the stagnation point $= X_s/a$
Y^*_s	dimensionless Y location of the stagnation point $= Y_s/a$

Greek symbols

δ_T	thermal boundary layer thickness at length L
ΔT	temperature difference between heated wall and bulk liquid $= T_w - T_m$
μ	dynamic viscosity
σ	surface tension of liquid
σ_T	linear coefficient of surface tension variation due to temperature
ρ	density
ψ^*_{min}	minimum stream function (ψ_{min}) non-dimensionalized by ψ_{ref}
ψ_{ref}	reference stream function $= \sigma_T \Delta T a/\mu_\ell$

Subscripts

g	gas
ℓ	liquid
m	bulk liquid
max	maximum
min	minimum
s	bubble surface
w	wall

In pursuit of knowledge about liquid motion in the vicinity of a bubble on a heated surface, research effort was initiated more than two decades ago. However, literature still remains scarce in this area. Consequently, even the rudimentary aspect of the problem is not yet well-understood, especially in a microgravity environment. In all the work carried out so far, the bulk liquid is considered to be stagnant initially. Larkin [8] carried out the first numerical study of thermocapillary flow around a hemispherical bubble placed on a solid wall subject to constant heat flux. He observed that the liquid is pulled towards the intersection of bubble and plate, then flows around the bubble surface and leaves the bubble as a jet. Kao and Kenning [9] extended the work of Larkin by taking into consideration the heat transfer through the bubble surface and the effect of gravity (natural convection). Their study showed that the interfacial heat transfer can be high in the case of a water–vapor system, whereas for a gas bubble–liquid system it is negligibly low. They observed that as the liquid jet penetrates into the bulk liquid, it creates an unstable density gradient within the liquid giving rise to a natural convection cell. They further reported from experiment that thermocapillary flow is extremely sensitive to surface contamination, especially for water. Raake et al. [10] conducted a similar experimental investigation with air bubble and silicone oil, which is insensitive to surface contamination. In their study of the liquid temperature and velocity fields near the bubble, they observed an oscillatory instability in the flow at a high temperature dif-

ference between the hot wall and bulk fluid. Their work was later extended to a higher temperature difference regime to observe steady, transitional and different modes of oscillatory motion [11,12]. Straub [13] also reported an experimental study of the phenomena using liquid–vapor systems of methanol, propanol, ethanol, R113 and water. The first reduced-gravity experiment on this subject was performed by Wozniak et al. [14]. In their ground-based experiment, they identified a co-existing mechanism of natural and thermocapillary convection governing the flow and temperature fields. In contrast, in the reduced-gravity environment of a sounding rocket, thermocapillary convection was observed to be the only transport mechanism. These experimental observations [12,14] were supplemented by numerical analysis, recently carried out by Kassemi and Rashidnia [15]. In all these previous works, the bulk liquid is considered to be quiescent initially, which resembles pool boiling.

Recent studies on pool boiling [16], forced convection boiling [17] and bubble formation in flowing liquid [18,19] under microgravity condition suggest the necessity of bulk liquid motion. With greatly reduced buoyancy in space, forces due to bulk liquid flow ensure a timely detachment of the bubble from the wall and thus control the bubble size. To improve the control aspect further, investigation is required to know if wall heating can be applied to alter the flow field around the bubble and the forces acting on it. Thereby, a combination of bulk liquid flow and wall heating can be utilized for the control purpose. Thus, it is important to understand the fluid motion near a bubble on a heated wall of a flowing liquid channel, i.e., in forced convection boiling configuration. Developing a knowledge base on the subject requires an extensive experimental and modeling work in microgravity. The present numerical work, as a starting step, investigates the fundamental fluid mechanics aspect of the problem.

Steady flow and temperature fields around a bubble on a heated wall in the presence of bulk liquid cross flow are numerically investigated, under microgravity condition. Two convection mechanisms are identified, namely thermocapillary convection and forced convection due to bulk liquid motion. It is shown that an interaction between these convection mechanisms governs the steady-state flow and temperature fields and shape of the deformable bubble. At the front side of the bubble facing the cross-flow, thermocapillary and forced convection cause liquid motion in the same direction, while at the downstream side they oppose each other, causing a recirculating flow there. Effects of the cross-flow velocity, length of the heated wall before the bubble, and temperature difference between the hot wall and the bulk fluid are investigated. The present study also investigates the role of these convection mechanisms in affecting wall heat transfer near the bubble.

2. Mathematical formulation

Fig. 1 shows the schematic of a channel of height h through which liquid of mean temperature T_m flows at an average velocity of U_{av}. For simplicity, the flow is assumed to be hydrodynamically fully developed and the velocity profile parabolic. One of the channel walls is maintained at a temperature T_w ($T_w > T_m$, $T_w - T_m = \Delta T$), while the other wall is insulated. Under microgravity condition, in the absence of body forces, the orientation of the heated wall (top or bottom heating) is not important. A gas bubble is injected into the liquid through a hole in the heated wall. Bulk liquid flow through the channel is perpendicular to the bubble axis ($x = 0$), which is a cross-flow configuration w.r.t. the bubble. Thus, the words channel flow and cross flow are used interchangably in this article. The liquid flow and ΔT create a thermal boundary layer which grows over length L to a thickness δ_T at the front end of the bubble. The thermal boundary layer in turn creates a temperature gradient dT/dt along the tangential direction of the bubble–liquid interface, leading to thermocapillary flow on and around the interface. Physical properties of the liquid, such as $\rho_\ell, \mu_\ell, c_{p\ell}$ and k_ℓ are assumed to be constant, except for σ which decreases linearly with temperature $[\sigma(T_2) = \sigma(T_1) - |\sigma_T|(T_2 - T_1), T_2 > T_1]$. Gas properties, μ_g and k_g, being much smaller than those of the liquid, are neglected.

Flow around a bubble (spherical or part of a sphere) due to combined forced and thermocapillary convection poses a three-dimensional problem. An accurate numerical modeling of a three-dimensional deformable free surface (bubble) is highly complex and computationally prohibitive. However, flow near the middle plane of the bubble (plane cut along the direction of forced convection) is approximately two-dimensional. Thus, knowledge about the important fluid mechanics aspect of this problem can be gathered qualitatively from a two-dimensional model, which is much less computationally involved. Therefore, in the present study we analyze a two-dimensional problem. During the bubble formation

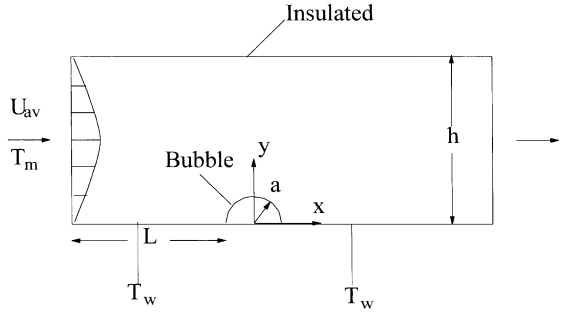

Fig. 1. Schematic of bubble on a heated wall with cross-flowing liquid.

period in boiling or other gas injection processes in liquid, bubble shape gradually changes from initially hemispherical to part of an approximate sphere and finally to nearly spherical at the point of detachment. At any instant during this formation time, the fundamental qualitative mechanics of the flow around the bubble, that is governed by the two modes of convection, remains the same. Our focus is on understanding the basic flow pattern and not on the details of the bubble shape influence on the flow. Therefore, we investigate the problem with the simplest geometry, i.e., a hemispherical bubble. The semi-circular bubble, illustrated in Fig. 1, is the two-dimensional equivalent of a hemispherical shape. During the computation, the semi-circular bubble is allowed to deform due to normal stress arising from bulk liquid motion and thermocapillary flow. In the presence of liquid cross-flow, the bubble tilts in the downstream direction. For high cross-flow velocity, angle between the wall and liquid meniscus at the downstream end of the bubble may become equal to the contact angle corresponding to the bubble, liquid and solid. The bubble loses its pinning edge at the downstream end in such a situation and the contact line starts to move along the wall [20]. Contact line behavior is a complex phenomenon by itself and is beyond the scope of this work. In this study, the cross-flow velocity ranges considered are small so that the bubble deforms, but remains pinned at the edge of the injection hole on the heated wall.

The governing equations are written in a normalized form, by non-dimensionalizing with respect to the following reference scales: length a, temperature $\Delta T\ (= T_w - T_m)$, velocity U_{ref} and pressure p_{ref}. The dimensionless continuity, momentum and energy equations, respectively, are:

$$\nabla \cdot \mathbf{u}^* = 0, \tag{1}$$

$$R_\sigma(\mathbf{u}^* \cdot \nabla \mathbf{u}^*) = -\nabla p^* + \nabla^2 \mathbf{u}^*, \tag{2}$$

$$(\mathbf{u}^* \cdot \nabla) T^* = \frac{1}{R_\sigma Pr} \nabla^2 T^*. \tag{3}$$

The governing equations are subject to the following boundary conditions:

$$\text{Hot wall} \quad \mathbf{u}^* = 0,\ T^* = 1. \tag{4}$$

$$\text{Insulated wall} \quad \mathbf{u}^* = 0,\ \partial T^*/\partial y^* = 0. \tag{5}$$

$$\text{Bubble surface} \quad u_n^* = 0, \tag{6}$$

$$p_g^* - p_\ell^* - \mu_\ell U_{ref}/(a p_{ref})(\partial u_n^*/\partial n^*) = \sigma/(a p_{ref} r^*). \tag{7}$$

$$\mu_\ell U_{ref}(\partial u_t^*/\partial n^*) = \mathrm{d}\sigma/\mathrm{d}t^* = \sigma_T \Delta T(\mathrm{d}T^*/\mathrm{d}t^*). \tag{8}$$

$$\partial T^*/\partial n^* = 0. \tag{9}$$

$$\text{Inlet at } x = -(\mathrm{L} + \mathrm{a})$$

$$u_x^+ = u_x/U_{av} = 6[(y/h) - (y/h)^2], \quad u_y^+ = 0. \tag{10}$$

Scaling of the shear stress balance equation (8) yields the reference velocity $U_{ref} = \sigma_T \Delta T/\mu_\ell$. Based on the reference velocity, the reference stream function ψ_{ref} in the vicinity of bubble is written as $\sigma_T \Delta T a/\mu_\ell$. The surface tension Reynolds number $R_\sigma\ (= \rho_\ell U_{ref} a/\mu_\ell)$, in Eq. (2), signifies the relative importance of inertia to viscous forces generated by thermocapillary action. The product of R_σ and Pr, commonly known as Marangoni number Ma, represents a ratio of heat transported by thermocapillary convection to that by conduction. For fixed liquid properties and bubble size, an increase in ΔT implies an increase in R_σ and Ma and thus a stronger thermocapillary convection. Forces arising from the bulk liquid motion in the channel also play a crucial role in the overall flow dynamics near the bubble. An important physical quantity characterizing this motion is the local channel flow velocity U_{loc} at bubble height a, written as $6U_{av}[(a/h) - (a/h)^2]$ for the assumed parabolic velocity profile. Local cross-flow Reynolds number $Re_{loc}\ (= \rho_\ell U_{loc}\ a/\mu_\ell)$ shows relative significance of inertia and viscous forces due to the bulk liquid motion near the bubble. The ratio of the two characteristic velocities U_{ref} and U_{loc}, termed here as velocity ratio $\bar{V}\ (= \sigma_T \Delta T/\mu_\ell U_{loc})$, can be considered to represent the relative importance of two viscous forces – generated by thermocapillary action and bulk liquid motion. This dimensionless parameter also signifies the ratio of heat transported by thermocapillary and forced convection. The tangential temperature gradient $(\mathrm{d}T/\mathrm{d}t)$ in Eq. (8), which governs thermocapillary motion, depends on the thickness of the thermal boundary layer created by wall heating and bulk liquid motion. The thermal boundary layer thickness is estimated at the front end corner of the bubble, developed over length L as $\delta_T \sim 5L/Re_L^{1/2} Pr^{1/3}$ [21]. Re_L is the Reynolds number based on U_{loc} and L. The ratio of thermal boundary layer thickness to bubble radius (δ_T/a) is another dimensionless parameter involved in this problem. In summary, the flow and temperature fields around the bubble are characterized by four dimensionless parameters, $R_\sigma, Re_{loc}, \delta_T/a$ and Pr, or in another form $\bar{V}, Re_{loc}, \delta_T/a$ and Pr. We use the latter group in this article as $\bar{V}$ gives a direct measure of the relative importance of thermocapillary and bulk liquid motion. For a fixed Pr, the number of dimensionless parameters reduces to $\bar{V}, Re_{loc}$ and δ_T/a. If the flow is viscous dominated, Re_{loc} does not have any effect on the overall flow field. In such a situation, only $\bar{V}$ and δ_T/a are sufficient to specify the transport fields.

To solve the problem numerically, a Spectral Element Method (SEM) based model is developed using computational fluid dynamics code NEKTON. NEKTON has been validated and proved to be very successful in modeling thermocapillary flow [22,23], coating flow [24], free surface flow in crystal growth [25] and 2-D laminar flow over a cylinder [26]. In SEM, the domain of interest is divided into a large number of unstructured elements, called spectral elements. Within each element the dependent variables are expanded in terms of high order

(4–14th) Legendre polynomials. The governing equations are written in variational form. Inserting Nth order polynomial expansions of the dependent variables into the variational form results in a set of discretized algebraic equations, which are solved using conjugate gradient method. Free surface tracking is decoupled from the bulk flow analysis by using Arbitrary Lagrangian Eulerian (ALE) method. The solution process starts with solving the discretized governing equations, subject to kinematic constraint (Eq. (6)) and tangential stress balance at the interface (Eq. (8)). The normal stress balance equation (7) is then utilized to determine the change in mesh co-ordinates on the free surface and the new free surface position. The change in the mesh co-ordinate is extended to the interior of the computational domain using an elastostatic mesh solver, thereby updating the geometry. Flow and temperature fields are resolved for the updated geometry and the procedure is repeated until the free surface geometry solution converges.

3. Results and discussion

Computations are carried out for 5 cs silicone oil ($Pr = 70$). This liquid is chosen as we plan to experimentally investigate the flow and temperature fields around the bubble using the same liquid. The surface tension of silicone oil is very low and is insensitive to contaminants. Thus, unlike an air–water system [9], thermocapillary flow in silicone oil is not affected by surface impurities. The parametric ranges considered are: $R_\sigma = 0$–162, $Ma = 0$–11340, $Re_{\mathrm{loc}} = 3.4$–10.2, $\bar{V} = 0$–47.4 and $\delta_T/a = 0.9$–1.5. Bubble size relative to the channel height (a/h) is kept constant at 0.17. Computations performed for other a/h ratios ($a/h = 0.06$–0.4) show that the transport fields around the bubble are independent of this parameter when all other parameters are kept constant. However, if the a/h ratio becomes close to 1, the flow pattern is drastically altered as the top wall is close to the bubble. Such geometric configuration is not considered in the present article. The capillary number based on the reference thermocapillary flow velocity ($Ca = \mu_\ell U_{\mathrm{ref}}/\sigma$) varies in the range of 7×10^{-5} to 0.09. This implies that the viscous normal stress due to thermocapillary motion is much less than the capillary stress and thus the bubble shape is not significantly deformed due to thermocapillary motion.

Before looking into the accuracy of the present numerical scheme, it is important to know the computationally critical region near the bubble. Therefore, the basic nature of the flow field is discussed before the grid independence study. At first, steady flow around a bubble is investigated for constant surface tension ($\sigma_T = 0, R_\sigma = 0$) condition, for $\Delta T = 5°C$ and $\delta_T/a = 1.5$. Thus there is no thermocapillary flow, i.e., this represents a purely forced convection case. For three different Re_{loc} conditions (3.4–10.2), the dimensionless velocity along the bubble surface ($V_s^+ = V_s/U_{\mathrm{loc}}$) is shown in Fig. 2. Dimensionless x location ($x^* = x/a$) of -1 represents the front end corner of the bubble facing the cross-flow, while $x^* = +1$ represents the downstream end corner. Surface velocities for the three Re_{loc} cases are compared with that for a purely viscous case, i.e., without the advection terms ($Re_{\mathrm{loc}} \to 0$). V_s^+ for the purely viscous case is symmetric about the bubble center axis ($x = 0$). Variation of V_s^+ between the viscous condition and the other Re_{loc} curves near the top of the bubble shows the effect of inertia due to bulk liquid motion. At the downstream end ($x^* > 0.5$), almost equal V_s^+ for the viscous and various Re_{loc} curves suggests that the flow is viscous dominated in this region. The viscous effect is observed to be less at the front end ($x^* < -0.5$), compared to that at the downstream end. Slight asymetry of V_s^+ between the front and downstream end for various Re_{loc} curves indicates the presence of a very weak wake effect at the downstream side. Due to the expanding geometry near the downstream end, the flow encounters an adverse pressure gradient in this region. However, the bubble surface flow momentum can overcome this gradient, ensuring that the bulk liquid follows the surface, without any separation. This is observed in the streamlines shown in Fig. 3(a) for the $Re_{\mathrm{loc}} = 3.4$ condition.

Fig. 3(b) illustrates the effect of thermocapillary convection. Keeping $\Delta T, U_{\mathrm{loc}}$ and δ_T same as in Fig. 3(a), surface tension along the bubble–liquid interface is varied with temperature ($\sigma_T \neq 0, R_\sigma = 27$) in Fig. 3(b). Due to a temperature gradient along the interface, surface tension is highest near the top of the bubble and

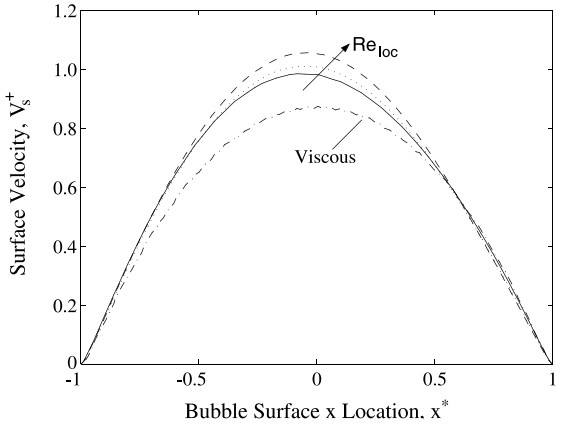

Fig. 2. Variation of surface velocity for pure forced convection cases ($\sigma_T = 0$) at constant $\Delta T = 5°C$ ($R_\sigma, \bar{V} = 0$). Comparison between $Re_{\mathrm{loc}} = 3.4, 6.8$ and 10.2 (corresponding δ_T/a values are 1.5, 1.1 and 0.9) cases with purely viscous flow condition.

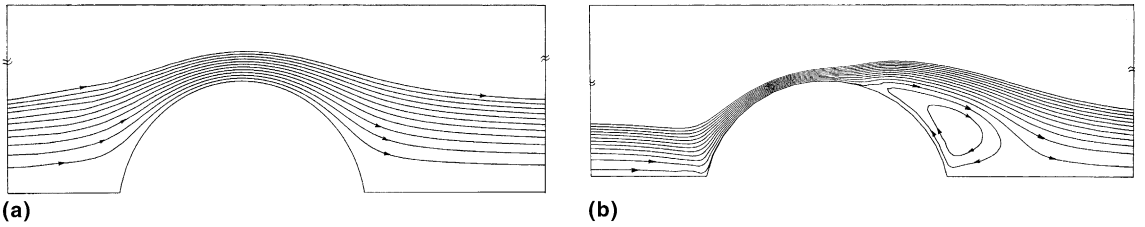

Fig. 3. Streamlines of steady flow field around a bubble for $U_{loc} = 8.3 \times 10^{-3}$ m/s $(Re_{loc} = 3.4), \delta_T/a = 1.5$ and $\Delta T = 5°C$. (a) $\sigma_T = 0, R_\sigma = 0, \bar{V} = 0$, (b) $\sigma_T = 0.0587 \times 10^{-3}$ N/m K, $R_\sigma = 27, \bar{V} = 7.9$.

lowest near the heated wall. This surface tension variation generates thermocapillary flow along the bubble surface, away from the hot wall towards the bulk liquid. At the upstream side of the bubble facing the cross flow, the bulk liquid motion and the thermocapillary effect create a free surface flow in the same direction. Thus flow near the front end of the bubble surface is governed by cooperating forced and thermocapillary convection. On the other hand, near the downstream end, the surface velocity due to bulk liquid flow and that due to thermocapillary flow are in opposite directions. The latter, being stronger among the two competing mechanisms, creates a reverse flow along the surface. The point on the bubble surface where the forward and reverse flow meet is termed as the stagnation point. The forward moving bulk liquid follows the bubble surface up to the stagnation point and separates thereafter. At the downstream end, as liquid moves up along the bubble surface due to thermocapillary effect, the surrounding liquid is pulled towards the hot corner to maintain continuity of liquid. Thus a recirculation cell is generated.

In order to resolve the flow and temperature fields accurately, a non-uniform spectral element grid is chosen with more number of elements near the bubble surface, especially in the recirculation region. Mesh dependence studies are carried out for $Re_{loc} = 3.4$, $R_\sigma = 162$ $(Ma = 11\,340, \bar{V} = 47.4)$ and $\delta_T/a = 1.5$, which represents the extreme condition in the present work. The most important parameters to judge grid independence are: minimum stream function of the recirculation cell $(\psi^*_{min} = \psi_{min}/\psi_{ref})$, minimum temperature on the bubble surface $(T^*_{s,min} = (T_{s,min} - T_m)/\Delta T)$, maximum bubble surface velocity in the direction of bulk liquid flow $(V^*_{s,max} = V_{s,max}/U_{ref})$, maximum reverse flow velocity on the bubble surface, which is minimum surface velocity as it is in the negative x direction $(V^*_{s,min} = V_{s,min}/U_{ref})$, the maximum cross-flow velocity within the channel $(U^*_{c,max} = U_{c,max}/U_{ref})$ and the x- and y-location of the stagnation point on the bubble surface $(X^*_s, Y^*_s = X_s, Y_s/a)$. Computations are performed for three different spectral element meshes with 142, 182 and 202 elements, each having 5th order polynomial expansion of the dependent variables. Comparison of the above parameters for these three meshes are shown in Table 1. Comparing the values in Table 1, the 182 element grid is chosen for all the computations.

Figs. 4(a) and (b) show the streamlines and isotherms for $Re_{loc} = 3.4, \delta_T/a = 1.5$ and $R_\sigma = 81$ conditions. Keeping U_{loc} same as in Fig. 3, ΔT is tripled in this figure to study the effect of wall heating. A comparison of Figs. 3(b) and 4(a) suggests that thermocapillary flow becomes stronger with an increasing temperature difference. At the front side of the bubble, thermocapillary action accelerates liquid flow along the bubble surface. To maintain continuity of liquid, the relatively colder bulk liquid is drawn towards the hot corner. This causes a slight bending of the near wall streamlines towards the hot corner (Fig. 4(a)) and clustering of isotherms in the region (Fig. 4(b)). At the downstream side, the recirculating flow penetrates deeper into the bulk fluid along the bubble surface and covers a wider area along the hot wall. Strengthening of the recirculating flow with increasing ΔT pushes the stagnation point on the bubble surface upstream. In the absence of cross-flow liquid velocity, thermocapillary flow is shown to be symmetric about the y axis, i.e., the stagnation point is located at $x = 0$ [8–15]. One may expect that with the additional motion of the cross-flowing liquid, thermocapillary effect will push the stagnation point towards the down-

Table 1
Grid independence for flow conditions, $Re_{loc} = 3.4, \delta_T/a = 1.5$ and $R_\sigma = 162$[a]

No. of elements	ψ^*_{min}	$T^*_{s,min}$	$V^*_{s,min}$	$V^*_{s,max}$	$U^*_{c,max}$	X^*_s	Y^*_s
142	−0.0230	0.5249	−0.0384	0.0737	0.0419	−0.8012	0.4170
182	−0.0229	0.5783	−0.0372	0.0781	0.0418	−0.8414	0.3663
202	−0.0229	0.5772	−0.0373	0.0784	0.0418	−0.8418	0.3658

[a] Corresponding $\bar{V} = 47.4$.

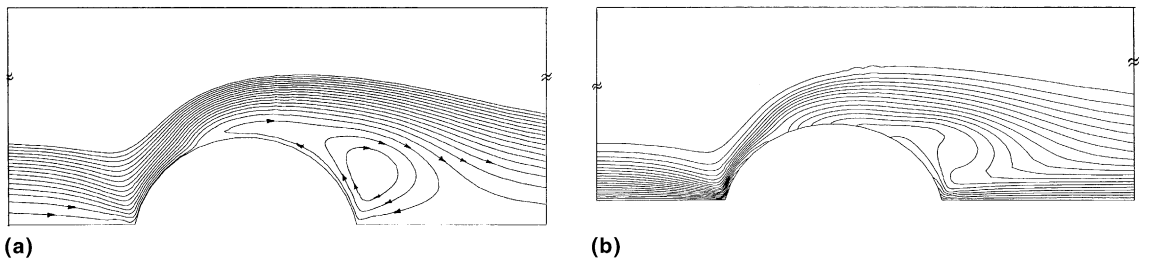

Fig. 4. (a) Streamlines and (b) isotherms for $Re_{loc} = 3.4, \delta_T/a = 1.5$ and $R_\sigma = 81$. Corresponding $\bar{V} = 23.7$.

stream end of the bubble. However, Fig. 4(a) suggests that at a high ΔT condition, the recirculation cell can have enough strength to cross over the line of symmetry towards the front end. An explanation of this phenomenon will be given later when we investigate the effect of ΔT on the surface temperature and velocity. The fact that the recirculating cell brings hot fluid up along the bubble surface is manifested by the upward bending of the isotherms at the downstream end, as observed in Fig. 4(b).

Variations of the dimensionless temperature T_s^* and velocity V_s^+ along the bubble surface are shown in Figs. 5(a) and (b), respectively, for three different sets of ΔT conditions. Re_{loc} is maintained constant at 3.4 and the δ_T/a ratio at 1.5. In order to understand the role of thermocapillary convection with increasing ΔT, the base condition is taken without thermocapillarity ($R_\sigma = 0$, as $\sigma_T = 0, \Delta T = 5°C$). Therefore, the only heat transfer mechanism in this case is forced convection. Bulk liquid motion tends to cool the surface, leading to a gradual drop in temperature from the front end hot corner along the bubble, as observed in Fig. 5(a). The other three curves in Fig. 5 represent non-zero σ_T cases, giving rise to thermocapillary flow. Thermocapillary effect dominates near the two corners, creating sharp temperature and velocity gradients there. At the front side, as thermocapillarity pulls liquid up along the surface from the hot corner, the surrounding colder liquid flows towards the corner to maintain continuity. This makes the thermal boundary layer thinner in the corner region, leading to a steeper temperature gradient with increasing R_σ, as shown in Fig. 5(a). In this region, the presence of thermocapillary effect brings in additional surface velocity in the same direction as bulk liquid cross-flow. As a result, with an increasing R_σ, a significant enhancement of surface velocity is observed in Fig. 5(b). Away from the front end corner, cooperating forced and thermocapillary flow governs the temperature profile and the former becomes increasingly important up along the surface. This leads to a gradual drop in surface temperature to the minimum point. Negative surface velocity in Fig. 5(b) underlines the presence of a reverse flow caused by thermocapillary convection from the downstream end hot corner. Thermocapillary effect dominates the temperature profile in this region, where the surface temperature varies from the minimum point to the wall temperature at the downstream end corner. The transition from positive to negative surface velocity represents

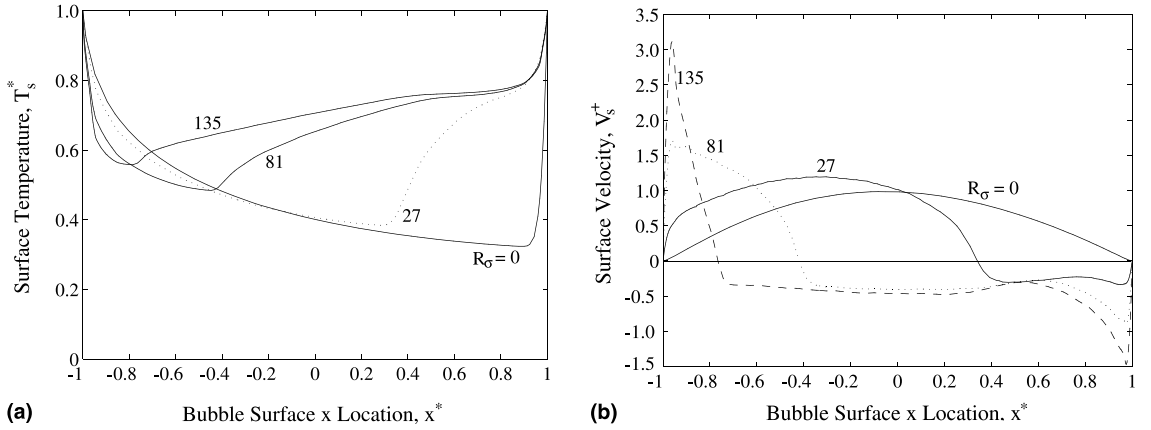

Fig. 5. Variation of (a) surface temperature and (b) surface velocity for different ΔT conditions at a fixed local cross-flow condition ($Re_{loc} = 3.4, \delta_T/a = 1.5$). Zero σ_T case: $\Delta T = 5°C$ ($R_\sigma = 0, \sigma_T = 0$). Non-zero σ_T cases: $\Delta T = 5°C$ ($R_\sigma = 27$), $\Delta T = 15°C$ ($R_\sigma = 81$), $\Delta T = 25°C$ ($R_\sigma = 135$). Corresponding $\bar{V} = 0, 7.9, 23.7$ and 39.5.

the stagnation point, where forward moving bulk liquid separates from the bubble surface. The stagnation point is observed to move upstream with increasing ΔT (R_σ). For an explanation of this phenomenon, we consider the surface temperature profile for $R_\sigma = 27$ in Fig. 5(a).

Surface temperature for $\Delta T = 5°C$ ($R_\sigma = 27$) is minimum at $x^* \sim 0.3$, which corresponds to the stagnation point in Fig. 5(b). As discussed earlier, just upstream (left) of this point, the temperature profile is governed by cooperating thermocapillary and forced convection. On the other hand, a sharp rise in temperature downstream (right) of this point marks the transition from the combined convection region to the thermocapillarity driven recirculation region, where the average liquid temperature is much higher than the bulk liquid. Keeping U_{loc} (Re_{loc}) constant, if ΔT (R_σ) is slightly increased from this point, thermocapillary driving force increases at both hot corners. At the front end corner, the temperature gradient becomes steeper and as a result, temperature along the front side of the bubble surface is lowered (Fig. 5(a)). In contrast, the average liquid temperature at the downstream side of the bubble goes up with ΔT. Lowering of surface temperature at the left side and its increase at the right side of the stagnation point lead to an increased temperature gradient in that region. This enhances the thermocapillary effect, which pushes the stagnation point upstream. At higher ΔT, the stagnation point goes even beyond the point of symmetry ($x = 0$), towards the front end corner.

How the interaction between thermocapillary and forced convection dictates the stagnation point is shown in Fig. 6. The dimensionless stagnation point ($X_s^* = X_s/a$), measured from the origin of the co-ordinate system, is plotted against $\bar{V}$. There is no separation of flow from the bubble surface when surface tension is constant ($\sigma_T, R_\sigma, \bar{V} = 0$), or the stagnation point is at the downstream end hot corner ($X_s^* = 1$). Along any Re_{loc} curve shown in Fig. 6, an increase in $\bar{V}$ implies a rise in ΔT, i.e., for fixed forced convection there is an increase in thermocapillary effect. A decreasing trend of X_s^* with $\bar{V}$ for all values of Re_{loc} in Fig. 6 shows that the stagnation point is pushed upstream with increasing thermocapillary effect, as discussed above.

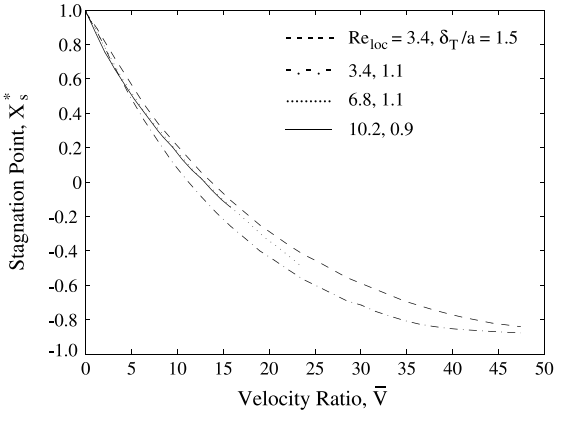

Fig. 6. Dimensionless separation point vs. velocity ratio for various local cross-flow Reynolds number and thermal boundary layer thickness conditions.

Effects of δ_T/a and Re_{loc} on the stagnation point are also investigated in Fig. 6. Keeping U_{loc} same as in the $Re_{loc} = 3.4, \delta_T/a = 1.5$ case, the length of the heated wall before the front end corner of the bubble (L) is halved ($Re_{loc} = 3.4, \delta_T/a = 1.1$). Comparing the two curves in Fig. 6, it is observed that at any $\bar{V}$ (same U_{loc} and ΔT conditions), the stagnation point is pushed further upstream for a thinner thermal boundary layer thickness. As the thermal boundary layer becomes thinner in the latter case, temperature at the front side of the bubble is lowered and the gradient at the front corner gets steeper, as seen in Fig. 5(a). On the other hand, the temperature profile at the downstream side remains unaltered by a change of δ_T. The increased temperature difference between the front and downstream side enhances reverse thermocapillary flow, thereby pushing the stagnation point upstream. Keeping δ_T/a constant, Re_{loc} is now doubled to investigate the role of inertia due to cross-flow velocity. A comparison of the $Re_{loc} = 3.4$, $\delta_T/a = 1.1$ and $Re_{loc} = 6.8, \delta_T/a = 1.1$ curves suggests that at any $\bar{V}$ condition, the stagnation point is pushed downstream with increasing Re_{loc}. At any fixed $\bar{V}$, moving from the $Re_{loc} = 3.4$ curve to 6.8 curve is equivalent to doubling of both ΔT and U_{loc}. Increasing ΔT tends to push the stagnation point upstream. On the other hand, surface velocity and forces in the direction of bulk liquid motion increase with U_{loc} (Fig. 2), which tends to push the stagnation point downstream. Of the competing effects, forces due to U_{loc} play a stronger role, thereby moving the stagnation point in its direction. Effects of these dimensionless parameters are further observed by a comparison of the $Re_{loc} = 3.4, \delta_T/a = 1.5$, $Re_{loc} = 6.8, \delta_T/a = 1.1$, and $Re_{loc} = 10.2, \delta_T/a = 0.9$ curves. Length L is kept constant in these computations. At any $\bar{V}$, moving from the $Re_{loc} = 3.4, \delta_T/a = 1.5$ curve to the $Re_{loc} = 6.8, \delta_T/a = 1.1$ curve implies doubling both ΔT and U_{loc} and thus reduction of δ_T/a for fixed L. As observed earlier, increased ΔT and reduced δ_T/a both enhance thermocapillary effect and tend to push the stagnation point upstream. The inertia and viscous forces due to U_{loc} do the reverse. In the present ranges considered, the change in the two opposing effects are almost equal, thereby keeping the stagnation point nearly constant.

It is further observed in Fig. 6 that for the $Re_{loc} = 3.4$ cases, X_s^* saturates to a nearly constant value (~ -0.8) at a high $\bar{V}$ condition. In the absence of liquid cross-flow, i.e., in an initially stagnant liquid case, thermocapillary convection alone generates two symmetric recirculation

cells at the two sides of bubble axis ($x = 0$) [8–15]. The stagnation point is located on the axis ($X_s^* = 0$). The present problem approaches the initially stagnant liquid case when ΔT is very high (mathematically $\Delta T, \bar{V} \to \infty$) or when U_{loc} is very small ($U_{loc} \to 0, \bar{V} \to \infty$). Due to limitations in computational grid and memory, the $\bar{V}$ condition in the present problem is restricted to a maximum value of 47.4. For the same $Re_{loc} = 3.4$ condition, if $\bar{V}$ could be increased well above the maximum value of 47.4 shown here, another recirculation cell will appear at the front end of the bubble. The beginning of this two cell (at the front and downstream end) flow pattern is observed in the streamlines corresponding to the $\bar{V} = 44.3$ ($Re_{loc} = 3.4, \delta_T/a = 1.5$ and $R_\sigma = 151$) condition, shown in Fig. 7. A strong suction effect causes the streamlines to bend towards the front end corner and thus the bulk liquid flow pattern is significantly altered. For ΔT conditions higher than that shown in Fig. 7, flow at the front end is expected to form a closed recirculation loop. Although the strength of the front end cell is less compared to that at the downstream end, it increases the temperature in that region due to recirculation. Thereby thermocapillary flow at the front end becomes stronger and consequently the stagnation point is slowly pushed back in the downstream direction. At very high $\bar{V}$ conditions ($\bar{V} \to \infty$), strength of the two recirculation cells becomes almost equal and X_s^* reaches 0. The saturation for $Re_{loc} = 3.4$ cases observed in Fig. 6 is actually the crest region of a higher $\bar{V}$ range plot.

Along with the stagnation point, another parameter that expresses the strength of the recirculation cell is its length along the heated wall (X_R). X_R (in dimensionless form $X_R^* = X_R/a$), measured from the downstream end hot corner, is plotted against $\bar{V}$ in Fig. 8. For a pure forced convection case ($\sigma_T, R_\sigma, \bar{V} = 0$), there is no recirculation cell, i.e., $X_R^* = 0$. Along any Re_{loc} curve, with an increase in $\Delta T(\bar{V})$ the thermocapillary flow gets stronger. Consequently the downstream end recirculation cell grows in size and its core region expands deeper into the channel. Thereby, the point at which the separated bulk liquid reattaches to the wall is pushed further away from the downstream end corner. This explains the rapidly increasing trend of X_R^* with $\bar{V}$ for all the Re_{loc} curves. It is further observed that the growth

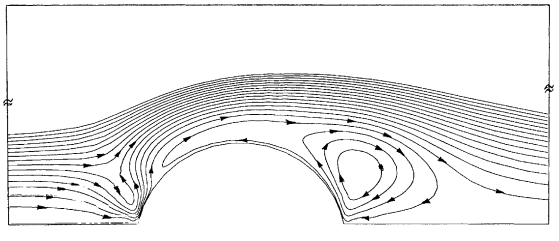

Fig. 7. Streamlines of flow around a bubble for $Re_{loc} = 3.4, \delta_T/a = 1.5$ and $R_\sigma = 151$. Corresponding $\bar{V} = 44.3$.

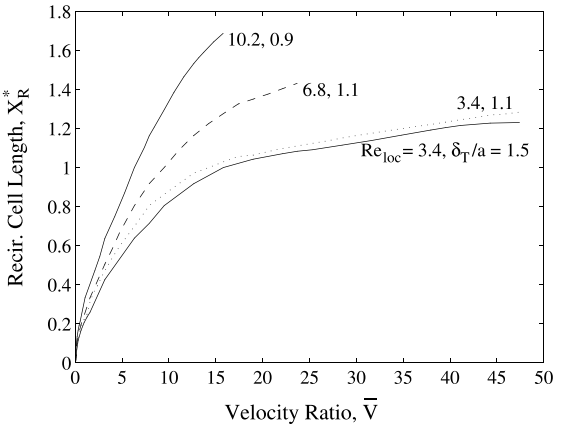

Fig. 8. Dimensionless length of recirculation cell vs. velocity ratio for various local cross-flow Reynolds number and thermal boundary layer thickness conditions.

rate of X_R^* is reduced at high $\bar{V}$. For $Re_{loc} = 3.4$ cases X_R^* eventually reaches a near constant value of beyond $\bar{V} \sim 40$. A comparison of Figs. 4(a) and 7 shows that at high $\bar{V}$, as the stagnation point crosses beyond the line of symmetry ($x = 0$) towards front end, expansion of the recirculation cell core slows down. As a result, the length of the recirculation cell does not grow significantly with $\bar{V}$.

Effects of δ_T/a and Re_{loc} are further investigated in Fig. 8. Keeping U_{loc} same as in $Re_{loc} = 3.4, \delta_T/a = 1.5$, L is halved so that δ_T/a is reduced to 1.1. As discussed earlier, thermocapillary flow at the downstream side gains strength with reduced δ_T/a. Consequently the recirculatory flow becomes stronger and the cell increases in size. Thus X_R^* is always higher for the lower δ_T/a case. In the next step, Re_{loc} is doubled from 3.4 to 6.8, keeping δ_T/a fixed at 1.1. At a fixed $\bar{V}$, both ΔT and U_{loc} are doubled between these two curves. As a result, the momentum of both the forward (bulk liquid) and reverse (thermocapillary) flow increase near the stagnation point. Consequently, the momenta of the detached bulk liquid motion and the return flow of the recirculation cell increase. This causes the bulk liquid to reattach to the wall at a distance further away from the downstream end corner. The increasing trend of X_R^* from $Re_{loc} = 3.4$ to 6.8 and 10.2 at any fixed $\bar{V}$ is thus explained.

The effect of thermocapillary flow on the local heat transfer coefficient at the wall is investigated in Fig. 9. x location along the heated wall and the local heat transfer coefficient (h_x) at that location are non-dimensionalized w.r.t. a.

$$Nu_x = \frac{h_x a}{k} = \frac{a}{(T_w - T_m)} \left| \frac{\partial T}{\partial y} \right|_{y=0}. \tag{11}$$

There is no heat transfer through the bubble surface, which corresponds to the region $-1 \leqslant x^* \leqslant 1$ in Fig. 9. Therefore, there are two branches in the Nusselt number

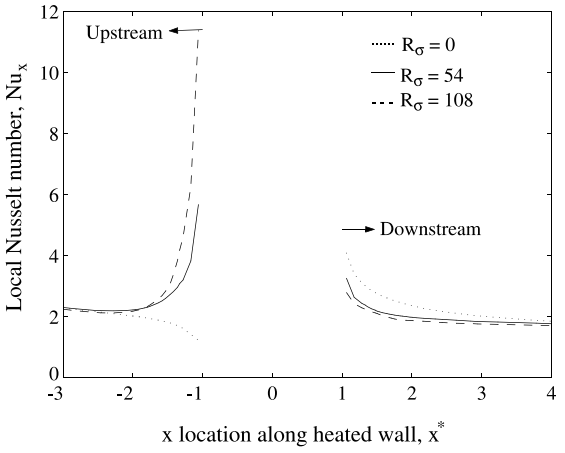

Fig. 9. Variation of local wall heat transfer coefficient for different ΔT conditions at a fixed local cross-flow velocity, $Re_{loc} = 3.4$. Zero σ_T case: $\Delta T = 10°C$ ($R_\sigma = 0$). Non-zero σ_T cases: $\Delta T = 10°C$ ($R_\sigma = 54$) and $\Delta T = 20°C$ ($R_\sigma = 108$). Corresponding $\bar{V} = 0, 15.8$ and 31.6.

plot. At first the bubble is treated as free surface without any thermocapillary effect ($\sigma_T = 0, \Delta T = 10°C, R_\sigma = 0$). At the upstream end, as the thermal boundary layer grows thicker with distance, heat transfer rate reduces, thereby showing a gradual decrease in the Nusselt number. After the insulated bubble surface, at the downstream end, a thermal boundary layer starts growing again from $x^* = 1$. As a result, the local heat transfer coefficient is higher in the starting region and slowly decreases with distance to a near constant value. The other two curves in Fig. 9, $R_\sigma = 54$ ($\Delta T = 10°C$) and $R_\sigma = 108$ ($\Delta T = 20°C$), represent non-zero σ_T cases. It is observed that at $x^* \sim -3$ and $x^* \sim 4$, Nu_x is approximately the same for all the cases. Thus $-3 \leqslant x^* \leqslant 4$ signifies the zone of influence of thermocapillary flow in terms of wall heat transfer. Within this distance range, it is observed that thermocapillary flow significantly alters the local wall heat transfer coefficient, especially at the upstream end. Thermocapillarity-induced suction effect at the front end of the bubble causes colder bulk liquid to flow towards the corner. Thus the thermal boundary layer becomes thinner, leading to enhanced heat transfer from the wall in this region. This explains the sharp rise in Nu_x curve near $x^* = -1$ for the $R_\sigma = 54$ and 108 cases, as compared to $R_\sigma = 0$. In contrast, at the downstream end thermocapillary effect reduces the heat transfer rate by a small amount. The recirculatory motion tends to increase the average liquid temperature at the downstream end by mixing of fluid, thereby reducing heat transfer from the wall.

4. Conclusion

Liquid motion on and near the surface of a gas bubble placed on a heated wall of a flowing liquid channel is investigated under microgravity condition. A two-dimensional numerical model is developed, based on spectral element method. It is shown that flow and temperature fields are governed by an interaction between thermocapillary convection arising at the bubble surface and forced convection due to bulk liquid flow. At the front end of the bubble facing the channel(cross) flow, two convection mechanisms assist each other, creating liquid motion along the surface away from the hot wall towards the top of the bubble. At the downstream end, thermocapillary action creates surface flow opposite to that created by bulk liquid motion. As a result, the forward moving liquid flow stagnates on the surface and separates thereafter. This sets in a recirculatory motion at the downstream end, strength of which is characterized by its length along the downstream side heated wall and location of the stagnation point on bubble surface. Channel flow velocity, temperature difference between the heated wall and bulk liquid and thermal boundary layer thickness (developed over the length of the heated wall before bubble) are identified to be the most important physical parameters. Increased temperature difference and thinner thermal boundary layer enhance thermocapillary effect and strengthen the recirculation cell. Consequently, the length of the recirculation cell increases and the stagnation point on bubble surface is pushed upstream towards the front end. Cross-flowing bulk liquid, on the other hand, pushes the stagnation point downstream and squeezes the cell in size. For fixed liquid properties, ratio of the cross-flowing bulk liquid inertia to viscous forces (local Reynolds number at bubble height), ratio of viscous forces due to thermocapillary motion and bulk liquid flow (velocity ratio) and ratio of thermal boundary layer thickness to bubble radius are observed to be important dimensionless parameters. It is further shown that heat transfer from the wall near the upstream end of the bubble is significantly increased due to thermocapillary effect, whereas a slight reduction takes place at the downstream end.

It is observed that wall heating significantly alters the flow field around the bubble. Thus the forces acting on the bubble, which govern its detachment from the wall, are also changed due to the presence of thermocapillary flow. This has an important implication in two-phase flow in space applications. It is proposed that a combination of heating and bulk liquid cross-flow can be utilized to precisely control bubble formation, size and frequency in the microgravity environment of space.

Acknowledgements

We gratefully acknowledge support from the National Aeronautics and Space Administration, Grant no. NAG3-1913, which made this work possible. We also wish to thank Dr. J. Masud and Mr. S. Gupta for useful discussion and help during this work.

References

[1] S. Banerjee, Space applications, Multiphase Flow and Heat Transfer: Bases and Applications Workshop, Santa Barbara, CA, 1989.
[2] E.T. Mahefky, Military spacecraft thermal management: The evolving requirements and challenges, in: Third AIAA/ASME Joint Thermophysics, Fluids, Plasma and Heat Transfer Conference (AIAA-82-0827), St. Louis, MO, 1982, pp. 3–16.
[3] P. Eckart, Spacecraft Life Support and Bio-spherics Life Support System, Kluwer Academic Publishers, Boston, 1996.
[4] A.E. Dukler, J.A. Fabre, J.B. McQuillen, R. Vernon, Gas–liquid flow at microgravity conditions: flow patterns and their transitions, Int. J. Multiphase Flow 14 (4) (1988) 389–400.
[5] H. Merte, Nucleate pool boiling in variable gravity, in: J.N. Koster, R.L. Sani (Eds.), Low Gravity Fluid Dynamics and Transport Phenomena, AIAA, Washington, DC, 1990. Prog. Astronaut. Aeronaut. 130 (1990) 15–69.
[6] J. Straub, M. Zell, B. Vogel, What we learn from boiling under microgravity, Microgravity Sci. Technol. 6 (1993) 239–247.
[7] S. Ostrach, Low-gravity fluid flows, Ann. Rev. Fluid Mech. 14 (1982) 313–345.
[8] B.K. Larkin, Thermocapillary flow around hemispherical bubble, AIChE J. 16 (1) (1970) 101–107.
[9] Y.S. Kao, D.B.R. Kenning, Thermocapillary flow near a hemispherical bubble on a heated wall, J. Fluid Mech. 53 (4) (1972) 715–735.
[10] D. Raake, J. Siekmann, C.H. Chun, Temperature and velocity fields due to surface tension driven flow, Exp. Fluids 7 (1989) 164–172.
[11] C.H. Chun, D. Raake, G. Hansmann, Oscillating convection modes in the surroundings of an air bubble under a horizontal heated wall, Exp. Fluids 11 (1991) 359–367.
[12] N. Rashidnia, Bubble dynamics on a heated surface, J. Thermophys. Heat Transfer 11 (3) (1997) 477–480.
[13] J. Straub, Transport phenomena in micro- and zero-gravitational fields, in: B.X. Wang (Ed.), in: Transport Phenomena Science and Technology, Higher Education Press, Beijing, China, 1992, pp. 16–28.
[14] G. Wozniak, K. Wozniak, H. Bergelt, On the influence of buoyancy on the surface tension driven flow around a bubble on a heated wall, Exp. Fluids 21 (1996) 181–186.
[15] M. Kassemi, N. Rashidnia, Steady and oscillatory flows generated by a bubble in 1-g and low-g environments, in: 35th Aerospace Sciences Meeting & Exhibit (AIAA 97-0924), Reno, NV, 1997.
[16] H.S. Lee, H. Merte, Hemispherical vapor bubble growth in microgravity: experiments and model, Int. J. Heat Mass Transfer 39 (12) (1996) 2449–2461.
[17] Y. Ma, J.N. Chung, An experimental study of forced convection boiling in microgravity, Int. J. Heat Mass Transfer 41 (15) (1998) 2371–2382.
[18] I. Kim, Y. Kamotani, S. Ostrach, Modelling bubble and drop formation in flowing liquids in microgravity, AIChE J. 40 (1) (1994) 19–28.
[19] A. Bhunia, S.C. Pais, Y. Kamotani, I. Kim, Bubble formation in a coflowing configuration in normal and reduced gravity, AIChE J. 44 (7) (1998) 1499–1509.
[20] H. Nahra, Y. Kamotani, Bubble formation and detachment in liquid flow under normal and reduced gravity, in: 36th Aerospace Sciences Meeting & Exhibit (AIAA 98-0732), Reno, NV, 1998.
[21] F.P. Incropera, D.P. DeWitt, Fundamentals of Heat and Mass Transfer, fourth ed., Wiley, New York, 1996, pp. 351–353.
[22] E.T. Bullister, L.W. Ho, E.M. Ronquist, A.T. Patera, Computational environment for microgravity materials processing simulations, Final report on NASA contract NAS3-26132, Phase I SBIR, Cleveland, OH, 1991.
[23] J. Masud, Y. Kamotani, S. Ostrach, Report no. EMAE 97-217, Department of Mechanical & Aerospace Engineering, Case Western Reserve University, Cleveland, OH, January 1997.
[24] K. Kumar, S. Subbiah, P. Murtagh, Numerical modeling of multilayer slot coating flows, in: P.H. Gaskell, M.D. Savage, J.L. Summers (Eds.), Proceedings of the First European Coating Symposium on the Mechanics of Thin film Coatings, World Scientific, Singapore, 1996, pp. 42–51.
[25] A.G. Ostrogorsky, Numerical simulation of single crystal growth by submerged heater method, J. Cryst. Growth 104 (1990) 233–238.
[26] NEKTON v 3.1.1 User's Manual and Training Notes, Fluent Inc., 1998.